ACS APPLIED MATERIALS & INTERFACES

Research Article

www.acsami.org

Gold Nanoshell-Decorated Silicone Surfaces for the Near-Infrared (NIR) Photothermal Destruction of the Pathogenic Bacterium *E. faecalis*

Orawan Khantamat,[†] Chien-Hung Li,[†] Fei Yu,[†] Andrew C. Jamison,[†] Wei-Chuan Shih,[‡] Chengzhi Cai,*[,†] and T. Randall Lee*[,†]

[†]Department of Chemistry and the Texas Center for Superconductivity and [‡]Department of Electrical and Computer EngineeringUniversity of Houston, Houston, Texas 77204-5003, United States

Supporting Information

ABSTRACT: Catheter-related infections (CRIs) are associated with the formation of pathogenic biofilms on the surfaces of silicone catheters, which are ubiquitous in medicine. These biofilms provide protection against antimicrobial agents and facilitate the development of bacterial resistance to antibiotics. The application of photothermal agents on catheter surfaces is an innovative approach to overcoming biofilm-generated CRIs. Gold nanoshells (AuNSs) represent a promising photothermal tool, because they can be used to generate heat upon exposure to near-infrared (NIR) radiation, are biologically inert at physiological temperatures, and can be engineered for the photothermal ablation of cells and tissue. In this study, AuNSs functionalized with carboxylate-terminated organosulfur ligands were attached to model catheter surfaces and tested for their effectiveness at killing adhered *Enterococcus faecalis* (*E. faecalis*) bacteria. The morphology of the AuNSs was characterized by scanning electron microscopy (SEM) and transmission electron microscopy (TEM), while the elemental composition was characterized by energy-dispersive X-ray spectroscopy (EDX) and X-ray photoelectron spectroscopy (XPS). Furthermore, optical and photothermal properties were acquired by ultraviolet−visible (UV-vis) spectroscopy and thermographic imaging with an infrared camera, respectively. Bacterial survival studies on AuNS-modified surfaces irradiated with and without NIR light were evaluated using a colony-formation assay. These studies demonstrated that AuNS-modified surfaces, when illuminated with NIR light, can effectively kill *E. faecalis* on silicone surfaces.

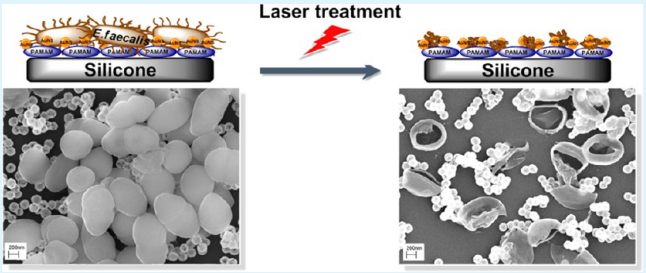

KEYWORDS: *gold nanoshells, catheter-related infections, polydimethylsiloxane, surface plasmon resonance, E. faecalis, photothermal*

INTRODUCTION

Because of the wide use of a variety of catheters in medical care, catheter-related infections (CRIs) are one of the most common types of nosocomial infections. CRIs are a major cause of patient morbidity and mortality, often leading to premature catheter replacement, along with the associated cost and patient discomfort. The use of peripheral venous catheters is responsible for most of the 200 000 nosocomial bloodstream infections that occur annually in the United States.[1] Catheter-related bloodstream infections have an attributable mortality rate of 10%−25% and an economic burden of up to $56 000 per episode.[2−4] Furthermore, catheter-associated urinary tract infections (CAUTI) account for ∼30% of the infections reported by acute care hospitals in the United States and affect millions of patients annually worldwide.[5−8]

Most indwelling catheters are made of silicone rubber. Bacterial adhesion and subsequent biofilm formation on the silicone surfaces is elemental to the onset of pathogenesis.[9] To prevent pathogenic colonization on silicone catheters and CRIs, a variety of approaches have been explored, but few have proven highly effective in the prevention of catheter-related infections.[10,11] In urinary tract infections, the use of antimicrobial agents either systemically or instilled directly into the bladder have been shown to be ineffective in preventing bacterial colonization.[11] Chronic antibiotic suppression of asymptomatic bacteria of a patient that is catheterized to prevent urinary tract infections leads to the emergence of resistant flora and adverse drug effects.[10] In short, innovative approaches are still required to limit exposure to, and proliferation of, these pathogenic micro-organisms on silicone surfaces.

Surface modification of catheters is generally required to inhibit biofilm formation and/or to eliminate bacterial infection from indwelling catheters. The application of metal nanoparticles, such as silver, on the surface of medical devices has been used as an antimicrobial route to prevent bacterial adhesion and subsequent biofilm formation.[12] However, the toxicity of silver nanoparticles toward mammalian cells has

Received: September 22, 2014
Accepted: January 22, 2015
Published: January 22, 2015

DOI: 10.1021/am506516r
ACS Appl. Mater. Interfaces 2015, 7, 3981−3993

Scheme 1. Strategy for Preparing AuNS-Modified PDMS Surfaces and Examination of their Efficacy in Killing Pathogenic *E. faecalis* Using NIR Illumination

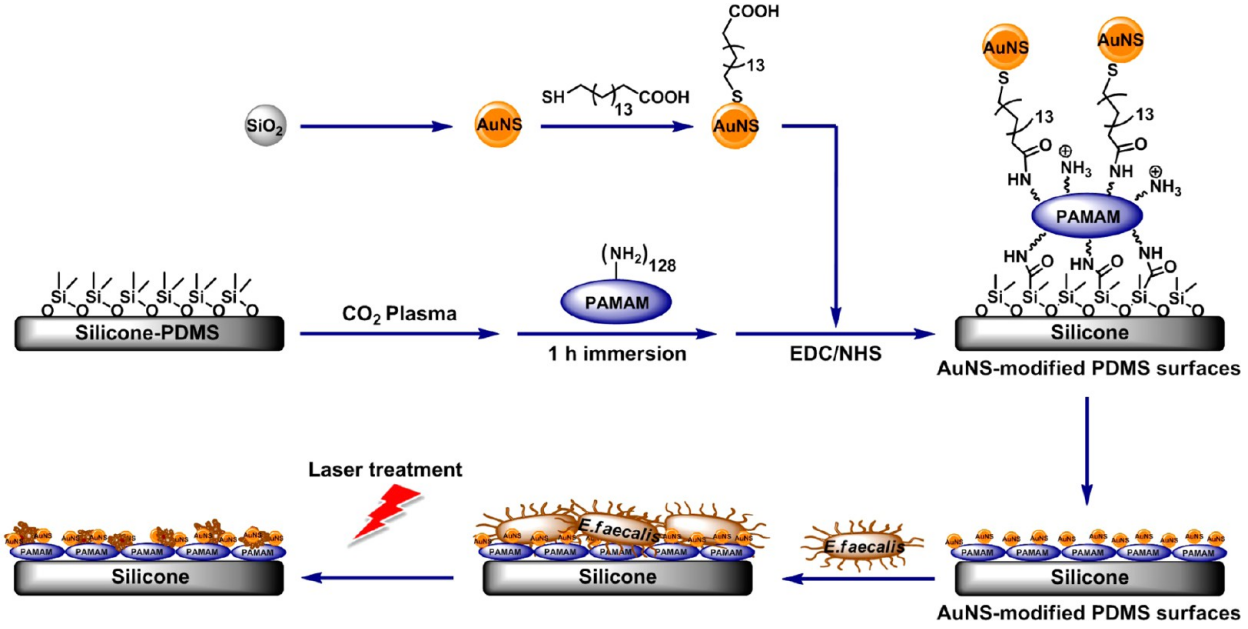

been reported by several groups,[13−15] and this concern limits their use in the surface modification of catheters. Another approach is the development of other types of metal nanoparticles as agents for the photothermal eradication of bacteria. Among the metal nanoparticles currently used in biological research, gold nanoshells (AuNSs), which consist of a thin gold shell surrounding a dielectric core, are strong candidates for this application.[16,17] AuNSs are biologically inert at physiological temperatures and can be engineered for photothermal ablation of cells and tissues via the heat generated by their strong surface plasmon resonance (SPR).[18,19] Localized SPR is a phenomenon in which light interacts with the conduction band electrons at the surface of a metal nanoparticle when the incident photons are in resonance with the collective oscillation of the electrons. For AuNSs, this property can be tuned through the manipulation of the dimensions of the dielectric core and the gold shell.[16,17] The toxicity of AuNSs has been examined, with all available evidence indicating that, at physiological doses, AuNSs are noncytotoxic and pose no short-term health risks.[18,19] Numerous *in vivo* studies in mice have provided the best evidence that AuNSs are not only nontoxic, but also safe, including a report where mice treated with AuNSs exhibited no clinical abnormalities or side effects months after treatment.[20]

AuNSs have been pursued as photothermal agents in medical applications because the SPR absorption band of these particles can be tuned from the visible (vis) region to the near-infrared (NIR) region. AuNSs that exhibit a strong SPR response when illuminated with NIR light at their resonance frequency convert the absorbed energy to heat as a means of dissipating that energy, which raises the hyperthermic stress of the targeted cells. In particular, the use of NIR light is most suitable for photothermal therapy because of its optimal penetration of body tissue due to the minimal absorption from tissue chromophores and water.[21]

Several reports have demonstrated the application of gold nanostructures in combination with their NIR absorption capacities in photothermia studies on animal cells[20,22−25] and bacteria.[26,27] In most of these cases, the gold nanostructures were suspended among the cells. However, the use of AuNSs as photothermal agents to modify catheter surfaces for killing bacteria under NIR irradiation has yet to be demonstrated, to the best of our knowledge, perhaps because (1) silicone catheters with their inert alkylsiloxane surface moieties are difficult to modify using this approach, and (2) bacteria are more resistant than animal cells to changes in temperature. However, these issues can be overcome if AuNSs can be made to attach directly to a model catheter surface, and the light-generated heat from the AuNSs is sufficiently lethal to adherent bacteria without causing irreparable damage to the surrounding tissue.

To this end, we developed a strategy for modifying polydimethylsiloxane (PDMS) as a model silicone catheter surface with carboxylic acid-terminated AuNSs engineered to absorb NIR light. Silicone rubbers are inert and hydrophobic polymers. Therefore, prior to attaching AuNSs, we first needed to activate the surface of the PDMS substrates. Previously, our research team reported an efficient method for introducing amino groups on PDMS surfaces, allowing for the attachment of a wide variety of molecules.[28] Herein, we use this strategy to effect the covalent attachment of carboxylic acid-terminated AuNSs as NIR photothermal agents. To prepare the nanoshells for this process, we coated them with a carboxylate-terminated organosulfur ligand, providing a means to form bonds with the amino groups of the model catheter surface. We employed a strain of drug-resistant *Enterococcus faecalis* (*E. faecalis*)—a ubiquitous uropathogen[29]—to demonstrate the feasibility of using AuNS-modified surfaces for killing pathogenic bacteria via NIR illumination. Scheme 1 illustrates the overall strategy developed in this study.

In the work reported here, we have used scanning electron microscopy (SEM), transmission electron microscopy (TEM), energy-dispersive X-ray spectroscopy (EDX), and X-ray photoelectron spectroscopy (XPS) to characterize the morphology and the elemental composition of the AuNSs, and we used UV−visible (UV−vis) spectroscopy to measure

DOI: 10.1021/am506516r
ACS Appl. Mater. Interfaces 2015, 7, 3981−3993

their optical properties. The photothermal properties of the AuNS-modified surfaces were analyzed using thermographic imaging with an infrared camera. Bacterial survival studies were conducted on AuNS-modified PDMS surfaces using a colony-formation assay both with and without NIR irradiation. Our results show significant potential for the development of AuNS-modified silicone surfaces as a means of killing nosocomial pathogens *in situ*.

EXPERIMENTAL SECTION

Materials. The following analytical-grade chemicals were purchased from the indicated suppliers and used without purification: tetraethyl orthosilicate, TEOS (98%, Aldrich); (3-aminopropyl)trimethoxysilane, APTMS (97%, Aldrich); tetrakis(hydroxymethyl)phosphonium chloride, THPC (80%, Aldrich); hydrogen tetrachloroaurate(III) hydrate, $HAuCl_4$ (49% Au, Strem Chemicals); potassium carbonate (Sigma–Aldrich); formaldehyde (35%–40%, Macron Fine Chemicals); 16-mercaptohexadecanoic acid, 16-MHDA (Aldrich); D,L-thioctic acid, D,L-α-lipoic acid (98+%, ACROS Organics); polydimethylsiloxane base and curing agent, PDMS (SYLGARD@ 184 Silicone Elastomer Kit, Dow Corning); octadecyltrichlorosilane, OTS (Alfa Aesar); Generation 5 (G5) poly(amidoamine) dendrimer (PAMAM; Dendritech); 1-ethyl-3-(3-(dimethylamino)propyl) carbodiimide hydrochloride, EDC (GL Biochem (Shanghai), Ltd.), *N*-hydroxysuccinimide, NHS (Aldrich); Luria–Bertani (LB) medium (BD Difco); tetracycline (Sigma); sodium dodecyl sulfate, SDS (J.T. Baker); and osmium tetroxide 4% aqueous solution (OsO_4; Electron Microscopy Sciences). Water was purified to a resistance of 18 MΩ·cm (Millipore water; Academic Milli-Q Water System, Millipore Corporation). All glassware was cleaned in an aqua regia solution (HCl:HNO_3; 3:1), thoroughly rinsed with Millipore water, and then dried prior to use.

Preparation of Gold Nanoshells. *Synthesis of APTMS-Functionalized Silica Nanoparticles.*[16,30] The silica nanoparticles were prepared by the base-catalyzed hydrolysis of TEOS using a slight modification of the Stöber method.[31] Briefly, absolute ethanol was mixed with ammonia solution (NH_4OH), and stirred at 800 rpm for 10–20 min. A subsequent aliquot of TEOS was added, and the solution was stirred overnight to obtain silica nanoparticles. The condensation of TEOS generally started within 10–15 min, which was easily observed by the change of the solution from colorless to opaque.

The silica nanoparticle surfaces were modified with APTMS to obtain NH_2 surface groups by adding 1 mL of APTMS to a 100-mL aliquot of the vigorously stirred silica nanoparticle solution. The mixture was allowed to react at room temperature for 1 h, and then gently refluxed for 3 h to enhance the covalent bonding of the APTMS groups to the silica nanoparticle surface. The APTMS-coated silica nanoparticles were isolated by centrifugation and redispersed in ethanol.

Synthesis of the Gold-Seeded Silica Particles. To attach colloidal gold particles to the APTMS-modified silica nanoparticles, we used a self-assembly method developed by Westcott et al.[32] The colloidal gold (1–3 nm diameter) solution was prepared by the reduction of a 1 wt % aqueous solution of $HAuCl_4$ with THPC.[33] Under rapid stirring, 1 mL of 1 M NaOH was added to 90 mL of Millipore water, followed by the addition of 2 mL of a 1.25% aqueous THPC solution. The reaction mixture was stirred for 5 min, and then 4 mL of 1 wt % $HAuCl_4$ in water was added quickly to the stirred solution. The colloid solution was stored at 4 °C for 2 days and then concentrated to 10 mL using a rotary evaporator.

A portion of the concentrated gold colloidal solution (5 mL) was then mixed with a 1 mL aliquot of APTMS-modified silica nanoparticle solution. After vigorous stirring for 1 h, the solution was allowed to equilibrate for 2 days to let the gold colloidal particles attach to the silica surface. The resulting seeded particles were then washed by centrifugation and redispersed in Millipore water.

Gold Nanoshell Growth. To grow the gold overlayer on the gold-seeded silica particles, a solution containing a reducible gold salt (K-gold solution) was first prepared by dissolving 25 mg of anhydrous potassium carbonate in 100 mL of Millipore water. After 10 min of stirring, 2 mL of 1 wt % $HAuCl_4$ solution in water was added. The solution initially appeared transparent yellow and slowly became colorless over the course of 30 min. The K-gold solution was then aged at 4 °C in darkness for a minimum of 2 days. The growth of the gold shell layers on the gold-seeded particles occurred through the deposition and reduction of Au^{3+} using formaldehyde.[16,32] To a vigorously stirred 4 mL aliquot of the colorless K-gold solution, the seeded particle solution was added, followed by adding 10 μL of formaldehyde. Over the course of 2–5 min, the solution changed from colorless to blue-green, which is characteristic of nanoshell formation. The nanoshells were separated from the solvent by centrifugation and decantation, and then redispersed in Millipore water.

Adsorption of Carboxylate-Terminated Organosulfur Species onto the Gold Nanoshells. The AuNSs were centrifuged and redispersed in 25 mL of ethanol (~2.5×10^9 particles/mL) prior to sparging with nitrogen gas for 30 min. Then, 25 mL of 10 mM carboxylate-terminated organosulfur ligand, either 16-MHDA or lipoic acid, in ethanol was added followed by continued stirring for 1 h. After allowing the mixture to react for 16–18 h at room temperature, the carboxylic acid-functionalized AuNSs were then washed by centrifugation to remove unreacted reagents and subsequently redispersed in Millipore water.

Preparation of AuNS-Modified PDMS Surfaces. *Preparation of the PDMS Substrates.*[28] A 10:1 ratio of PDMS base and curing agent were mixed thoroughly and allowed to stand for at least 30 min, until no bubbles were visible in the mixture. To prepare a thin layer of PDMS, the mixture was gently poured on top of a clean silicon wafer and then pressed against an OTS-modified silicon wafer. The purpose of using an OTS film was to aid in the peeling of the top silicon layer to expose a relatively flat PDMS surface. After the mixture was cured at 110 °C overnight, the PDMS was removed from the OTS-modified silicon wafer template, and the PDMS surface was rinsed with Millipore water and dried with argon gas. The PDMS substrate was then cut into 0.3 cm × 1 cm pieces to be used in the next step of the procedure.

Preparation of the PAMAM-Modified PDMS Surface. Oxidation with a CO_2 plasma was carried out on the PDMS surface using a Harrick plasma cleaner (Model PDC-32G, 100 W) at a low power setting (6.8 W). The PDMS surfaces were exposed to CO_2 plasma for 45 s.[28] The resulting oxidized PDMS was immediately immersed in a solution of 1 mg/mL of G5 PAMAM dendrimer in phosphate buffered saline (PBS) for 1 h to provide the PAMAM-coated surface. All the PAMAM-coated surfaces were washed with copious amounts of Millipore water and dried with argon gas.

DOI: 10.1021/am506516r
ACS Appl. Mater. Interfaces 2015, 7, 3981–3993

Coupling of Carboxylic Acid-Terminated AuNSs to PAMAM-Modified PDMS Surfaces. The PAMAM-coated surfaces were placed in separate wells in a 24-well plate. A 0.5 mL aliquot of a Millipore water solution containing ~1.6×10^9 particles/mL 16-MHDA- or lipoic acid-functionalized AuNSs, 60 mM of EDC, and 30 mM of NHS was used to immerse each of the PAMAM surfaces for 2 h. After 2 h, the substrates were washed with Millipore water and dried with argon gas to produce the AuNS-modified PDMS surfaces.

Bacterial Culture Treatment and Photothermolysis with AuNS-Modified Surfaces. *Preparation of Bacterial Strains.* For all bacterial assays, a single colony from the pathogenic bacteria, a human bloodstream isolate of *E. faecalis*, was grown in 25 mL of LB media containing an appropriate antibiotic: 4 μg/mL tetracycline. After incubation overnight, the optical density at 600 nm (OD_{600}) was adjusted to 0.25 for the bacterial culture, corresponding to a bacterial concentration of 10^8 CFU/mL.

Adherence Assay of E. faecalis. The ability of *E. faecalis* to adhere to the AuNS-coated and noncoated PAMAM surfaces was assessed visually using a microscope. Each surface was placed in a separate well in a 24-well plate containing 1 mL of *E. faecalis* in LB media at a concentration of 10^8 CFU/mL. The surfaces were incubated with the bacteria for 120 h at 37 °C. After incubation, the surfaces were rinsed three times with PBS, and then imaged using a 40× objective lens of a Nikon 80i microscope (Nikon Instruments, Melville, NY).

Photothermal Study of AuNS-Modified PDMS Surfaces against E. faecalis. To conduct photothermal studies, the AuNS-modified PDMS surfaces were placed in separate wells in a 24-well plate containing 1 mL of *E. faecalis* in LB media at a concentration of 10^8 CFU/mL. The surfaces were incubated with the bacteria for 120 h at 37 °C. After incubation, the surfaces were rinsed with PBS and then irradiated with a diode laser (AixiZ model HLM5768120, CW 800 mW, 810 ± 10 nm) at a power of 2.5 W/cm^2 for either 0, 5, 7, or 10 min. Standard plate-based counting was performed on illuminated surfaces to obtain the count of the viable bacteria for the remaining *E. faecalis*. Briefly, the surfaces, after being rinsed with PBS, were transferred to a 1 mL solution of 0.01% SDS. The surfaces were then sonicated using a Bransonic ultrasonic cleaner (50 Hz, 80 W) for 10 min and subsequently vortexed at 2000 rpm for 2 min. Serial dilutions from the sonicated bacterial suspension (10^{-2}, 10^{-4}, and 10^{-6}) were prepared and 10 μL of each dilution was plated in duplicates on LB agar containing 4 μg/mL tetracycline. The plates were incubated at 37 °C, and the bacterial colonies formed were counted after 24 h.

Bacterial Morphology Determination Using SEM. Monitoring of the bacterial morphology on the AuNS-modified PDMS surfaces was conducted by SEM examination before and after exposure to NIR light. In brief, the surfaces were fixed with 2.5% glutaraldehyde for 18 h, and then washed with PBS. The sample surfaces were further postfixed with 1% OsO_4 for 2 h, washed with PBS, and then dehydrated in an ascending ethanol series (50%, 70%, 85%, 95%, and 100%) for 10 min each. Finally, the samples were placed in 100% *t*-butanol for 20 min, followed by freeze-drying using a Scanvac CoolSafe 110-4 (LaboGene). The freeze-dried samples were then sputter-coated with platinum (Hummer 6.2 Sputter System; Anatech USA) and then examined by SEM.

Thermal Imaging Experiments. A PDMS surface modified with gold nanoshells was irradiated for 10 min using a diode laser (AixiZ model HLM5768120, CW 800 mW, 810 ± 10 nm). The thermal maps were acquired from the side of the surface on which the AuNSs were deposited. The thermal images were acquired using a thermographic infrared camera (ThermoVision A320G; FLIR Systems) with thermographic acquisitions conducted for 5 s.

Characterization Methods. The size and morphology of the AuNSs was characterized by scanning electron microscopy (SEM) (LEO, Model 1525), operating at an accelerating voltage of 15 kV, and transmission electron microscopy (TEM) (JEOL, Model 2000 FX), operating at 200 kV. To obtain high-resolution images from the SEM analysis, all samples were deposited on a silicon wafer and allowed to dry. For the TEM analyses, the AuNSs were deposited on a 300-mesh holey carbon-coated copper grid and allowed to dry. The DLS data were collected using an ALV-5000 Multiple Tau Digital Correlation instrument operating with a 514.5-nm light source at a fixed scattering angle of 90°. The sample diameters measured by DLS were consistent with the values obtained by SEM and TEM. The SEM images were processed using the Java-based "ImageJ" program, and the size histograms were constructed from an analysis of at least 150 particles.

The chemical composition of the AuNSs was analyzed by energy-dispersive X-ray (EDX) spectroscopy using an Oxford EDX attached to the SEM microscope. To determine the surface charge of the AuNSs, the zeta potential was measured with a Nicomp 380 ZLS from Particle Sizing Systems. The surface chemistry of the AuNSs was examined by X-ray photoelectron spectroscopy (XPS) (PHI Instruments, Model 5700 XPS) equipped with a monochromatic Al Kα X-ray source. UV−vis spectra were obtained using a UV−vis spectrometer (Cary, Model 50 Scan) over the wavelength range of 300−1000 nm. To prepare the bacterial samples for SEM imaging, the samples were freeze-dried using the procedure described above.

RESULTS AND DISCUSSION

Preparation and Characterization of AuNSs. To prepare the AuNSs used in this study, we first generated silica core particles using the Stöber method. Such silica nanoparticles can be fabricated by a variety of methods,[31,34−37] but the favored synthesis route for silica particles remains the Stöber method and its modifications.[38,39] This procedure allows the production of spherical and homogeneous silica particles of a desired size without the use of sophisticated equipment. Since this work requires that the AuNSs exhibit a photothermal response specifically to NIR light, the monodispersity of the core particles, along with their composition and size, are crucial concerns for the preparation of AuNSs having a desired absorption/scattering profile. In our study, we synthesized nanoparticles with dielectric silica cores ~145 nm in diameter. The functional groups at the surface of a typical unmodified silica nanoparticle are predominantly silanol (Si−OH) or ethoxy (Si−OEt) groups.[40] To enable synthesis of the nanoshell, the silica particles were functionalized with APTMS to create a layer of surface amino groups that allow for the attachment of colloidal gold.

Fabrication of the gold shells on the silica cores was accomplished using the seeded-growth method, a process which allows for good control of the shell thickness and surface properties. With this method, the APTMS-functionalized silica nanoparticles are initially decorated with colloidal particles of gold (1−3 nm). The gold colloids formed by the reduction of $HAuCl_4$ with THPC have a net negative surface charge,[38]

DOI: 10.1021/am506516r
ACS Appl. Mater. Interfaces 2015, 7, 3981−3993

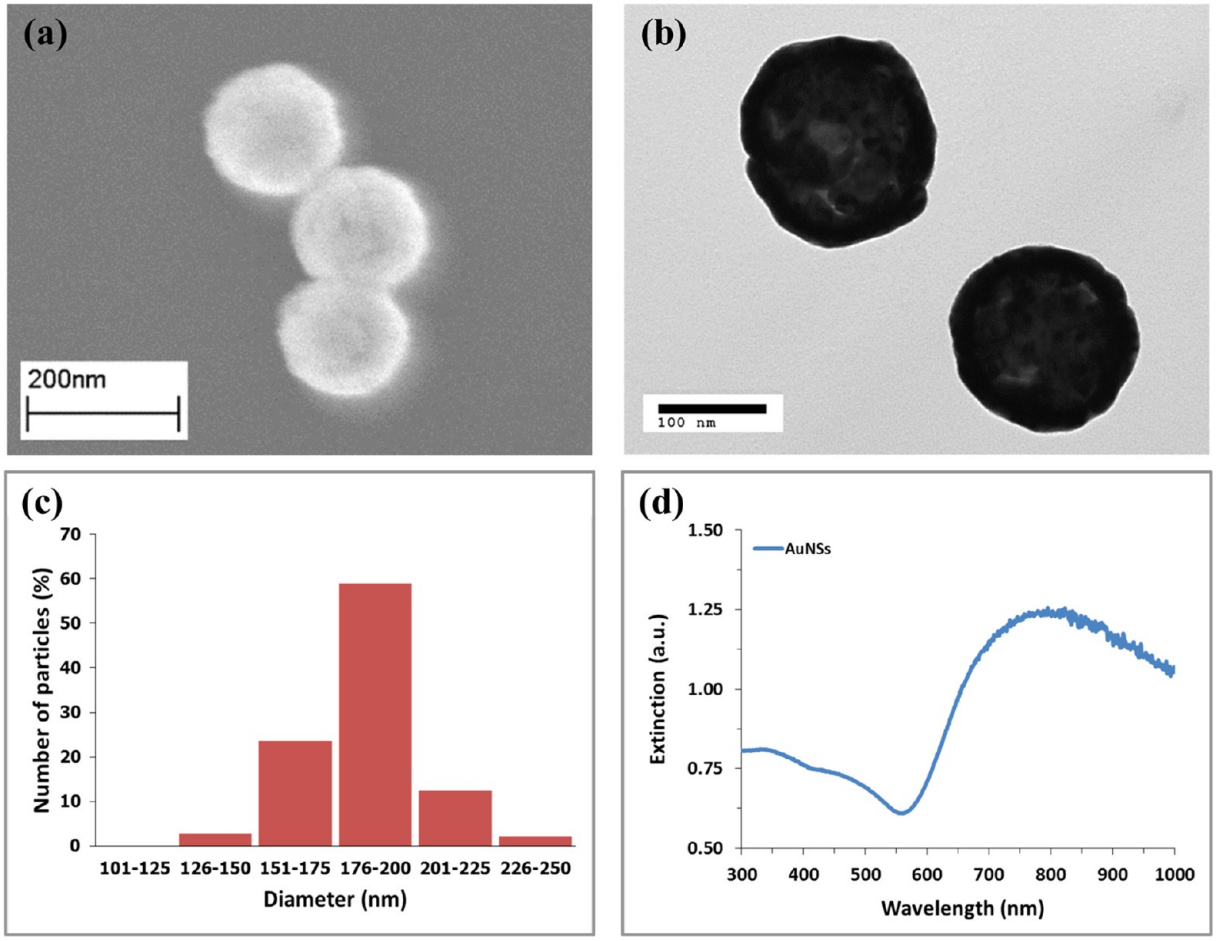

Figure 1. Morphology of the AuNSs as revealed by (a) SEM and (b) TEM images. (c) The size distribution of the AuNSs and (d) the extinction spectrum of the AuNSs in water.

leading to their attachment to the amino groups on the silica sphere, which are positively charged at neutral pH. In the final step of the formation of the shell, the attached gold nanoseeds are used to nucleate the growth of a gold overlayer to form the AuNS in the presence of $HAuCl_4$ and the reducing agent, formaldehyde. Figures 1a and 1b show SEM and TEM images, respectively, of the synthesized AuNSs exhibiting a uniform shell layer of ∼20 nm. The gold coating is continuous with topographical roughness on a nanometer scale. The particle size distribution of the AuNSs determined from the SEM images is shown in Figure 1c, and the associated average diameter is 185 ± 19 nm, which is a value that is consistent with those obtained via TEM and DLS measurement.

The optical response of the gold nanoshells can be adjusted by varying the relative core size and shell thickness, which is an aspect of this research that can be roughly verified by observing the color of the gold nanoshell solution during synthesis. These synthetic parameters can be used to vary the SPR absorption band across a broad range of the optical spectrum from the visible to the NIR spectral regions.[41] To analyze the extinction spectrum of our AuNSs, we collected a UV−vis spectrum over the wavelength range of 300−1000 nm, as shown in Figure 1d. Our AuNSs exhibit an absorption maximum at ∼800 nm, aligning with the emission wavelength of the diode laser used in the photothermolysis study.

We employed EDX to determine the chemical composition of the silica/gold core/shell nanoparticles. The EDX spectrum (see Figure S1 in the Supporting Information) confirms the presence of Au with peaks at 2.12 and 9.71 keV (Mα and Lα, respectively), Si with a peak at 1.74 keV (Kα), and O with a peak at 0.53 keV (Kα). These data are consistent with the expected composition of the AuNSs. In addition, the EDX-derived atomic composition data for the AuNSs is provided in Table S1 in the Supporting Information, including the atomic percentages of 51.1, 17.8, and 31.2 for O, Si, and Au, respectively.

We also performed a zeta potential measurement, using a Nicomp Model 380 ZLS device, to determine the surface charge on our AuNSs in aqueous solution. The average charged surface for the AuNSs was −43.2 ± 0.6 mV, which indicates that there is a negative charge distribution on the gold shell. The large value for the zeta potential is consistent with a model in which the presence of charges on the surface confers stability to the AuNSs in aqueous solution, preventing their aggregation and precipitation. Furthermore, the negative charge of the AuNS surface can be attributed to the presence of formate ligands that were present during the growth of the shell (*vide infra*).[30,42,43]

The surface composition of the AuNSs was analyzed by XPS. Figure S2a in the Supporting Information shows a high-resolution XPS spectrum for the Au 4f binding energy (BE) region, with the lower energy peak being used as a reference peak for our spectrum at 84.0 eV. The XPS spectrum highlighting the C 1s binding energies for the AuNSs in Figure

DOI: 10.1021/am506516r
ACS Appl. Mater. Interfaces 2015, 7, 3981−3993

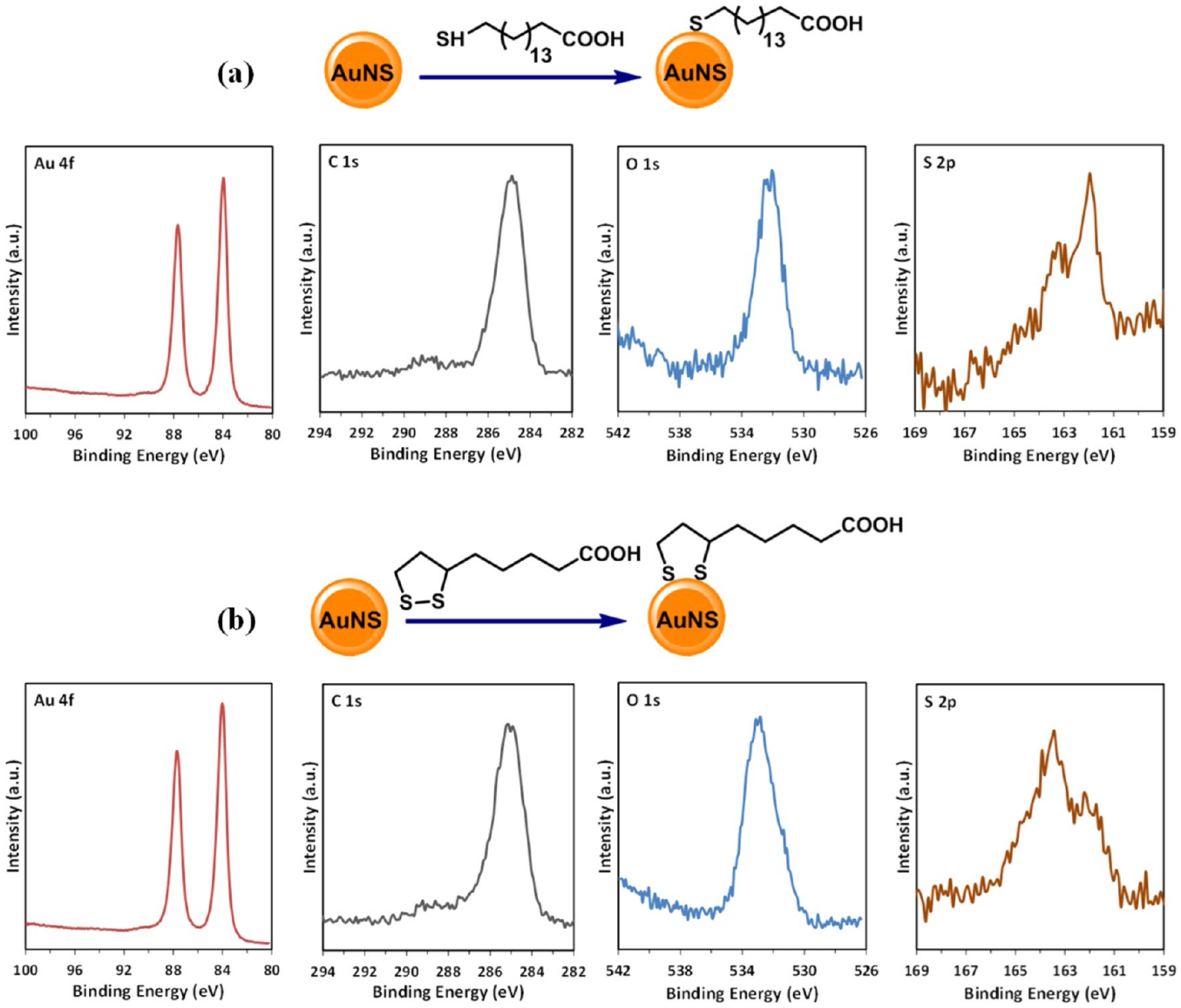

Figure 2. Schematic of the adsorption of (a) 16-MHDA and (b) lipoic acid onto a AuNS. In addition, the XPS spectra for 16-MHDA- and lipoic acid-functionalized AuNSs are included for the spectral regions of the Au 4f, C 1s, O 1s, and S 2p binding energies.

S2b in the Supporting Information exhibits three noteworthy signals: the peaks at ~284.6 eV (attributed to C−C/C−H bonds), at ~286.2 eV (associated with C−O bonds), and at ~288.5 eV (attributed to O═C−O species).[42] Figure S2c in the Supporting Information shows that the O 1s peak appears at ~533.1 eV, which is the binding energy that is associated with the C−O bond.[42] These results are consistent with the adsorption of formate molecules on the surface of the nanoshells.[30,42,43]

Adsorption of Carboxylate-Terminated Organosulfur Species onto the AuNSs. To use the AuNSs as photothermal agents for modifying model catheter surfaces, we initially generated carboxylic acid-terminated AuNSs by chemisorption. In previous studies, the self-assembly of thiol molecules has proven to be a simple and useful means of functionalizing metal nanoparticles.[44] In the present report, two types of carboxylate-terminated organosulfur species were used to generate surfaces that were functionalized with carboxylic acid/carboxylate groups: 16-MHDA and lipoic acid. Such terminally functionalized adsorbates have often been utilized for engineering interfaces involving proteins, nucleic acids, and other biomolecules because of the versatility of the COOH terminal group for covalent functionalization.[45−48] These molecules, with a polar terminal group, are capable of imparting solubility in aqueous systems via electrostatic stabilization, rendering them desirable for the current study. Moreover, the biocompatibility of lipoic acid makes it attractive for use in biological systems.

We used XPS to confirm the covalent attachment of these carboxylate-terminated organosulfur ligands onto the surfaces of the AuNSs. Figure 2 shows the XPS spectra of 16-MHDA- and lipoic acid-functionalized AuNSs. The Au 4f, C 1s, and O 1s BE regions of the spectra obtained for both modified AuNSs are similar from one figure to the next and are otherwise unremarkable. The S 2p spectra of the modified AuNSs can be deconvoluted using the S 2p doublet with a branching ratio of 1:2 and an energy difference of ~1.2 eV.[49] This analysis reveals that two species are predominant on the gold surface: thiolate bound to gold, with S $2p_{3/2}$ (S $2p_{1/2}$) at 161.9 eV (163.1 eV), and unbound sulfur in the form of thiol or disulfide, with S

DOI: 10.1021/am506516r
ACS Appl. Mater. Interfaces 2015, 7, 3981−3993

$2p_{3/2}$ (S $2p_{1/2}$) at 163.3 eV (164.5 eV).[49] The BEs for the S $2p_{3/2}$ of the 16-MHDA-functionalized AuNSs are ~162 eV, indicating that all of the adsorbates are bound thiolate with no unbound thiol or disulfides. In contrast, the lipoic acid-modified AuNSs exhibit, upon deconvolution, an S $2p_{3/2}$ peak at ~161.9 eV for bound thiolate and an S $2p_{3/2}$ peak for unbound thiol and disulfide at ~163.6 eV. The ratio of bound to unbound thiol/disulfide is 1:1.3. Other than the possible rupture of both disulfide S−Au bonds to the surface, the presence of unbound sulfur moieties might be due to carboxylic acid dimers; alternatively, some molecules might be attached to the surface through hydrogen bonding between the carboxyl ends.[50]

In addition, the modification of the AuNSs with a coating of either carboxylate-terminated organosulfur species yields a dispersion of particles that exhibits an invariant extinction spectra profile for all nanoshells, with the surface plasmon resonance peak centered at ~800 nm (see Figure S3 in the Supporting Information). These data indicate that the adsorption of either thiol compound will exert little or no influence on this key light absorption/scattering characteristic and, presumably, the associated photothermal properties.

Preparation and Characterization of AuNS-Modified PDMS Surfaces. To prepare the AuNS-modified model catheter surfaces for photothermal studies, the AuNSs were attached to the PDMS surfaces using our previously reported method.[28] In the literature, the most common method for activating silicone surfaces is based on the use of oxygen plasma to oxidize the organic component of the polymer, leaving a hydrophilic silicon oxide layer on the surface. The attachment of the desired functional moieties on the surface is usually accomplished via a siloxane intermediate layer terminated with an amino group, to which the functional moieties are tethered via amidation. In addition to this cumbersome multistep procedure requiring careful control of the siloxane chemistry, the major drawback of this approach is associated with the limited stability of the siloxane films.

Our method overcomes these limitations. Specifically, we use a mild CO_2 plasma instead of an O_2 plasma for activating the silicone surfaces, which greatly decreases the degradation of the silicone polymer and generates polar groups such as carboxylic acids, aldehydes, and hydroxyl groups, for subsequent functionalization. In addition, to reduce the loss of active groups on the surface via diffusion of the degraded polymers, we treated the surface immediately after CO_2 plasma exposure with a polyamine, such as the amino-terminated G5 PAMAM dendrimer possessing ~128 peripheral amino groups,[51] which cross-link with the active groups to generate a high density of amino groups on the surface for subsequent biofunctionalization. Using this procedure, we showed that the PAMAM-presenting surfaces were stable for over a month in PBS at 37 °C.[28]

To demonstrate the adhesion of the AuNSs on the PAMAM-coated surface, the carboxylic acid-terminated AuNSs were coupled to the surfaces via amidation in the presence of activating agents EDC and NHS. Figure 3 provides SEM images of the surfaces that show the distribution of the AuNSs on the PDMS with a surface coverage of 30%−35% (~1.3×10^9 particles/cm^2). Interestingly, we found that the bare AuNSs can absorb on the PAMAM-coated surfaces with immobilization upon exposure to the bare AuNS solution for 6 h without EDC/NHS (see Figure S4 in the Supporting Information). Although the nature of the bonding of the bare AuNSs on the samples prepared without EDC/NHS remains unclear, it plausibly occurs via an an electrostatic interaction between negative charges of the formate moieties on the AuNSs and positive charges of the amino groups on the PAMAM periphery.

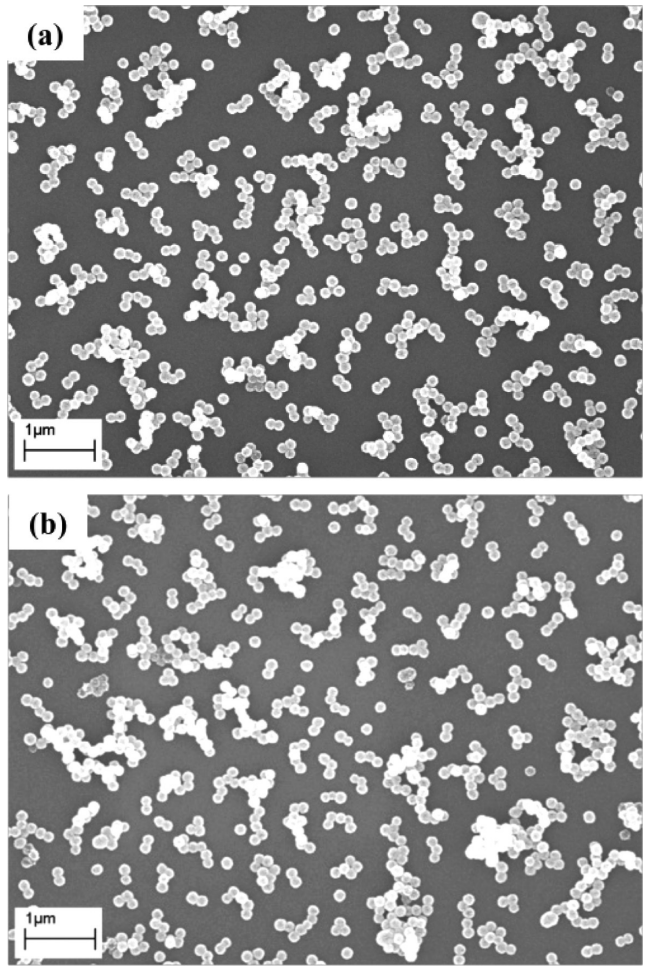

Figure 3. SEM images of AuNS-modified PDMS surfaces with (a) 16-MHDA-functionalized AuNSs and (b) lipoic acid-functionalized AuNSs.

We also used XPS to confirm the successful conjugation of the AuNSs to the PDMS substrate. Figures S5, S6, S7, and S8 in the Supporting Information show the XPS spectra of the PDMS surface, PAMAM-modified PDMS surface, and AuNS-modified PDMS surface with 16-MHDA- and lipoic acid-functionalized AuNSs, respectively. The spectral data are consistent with the expected composition of the surfaces. In addition, the PDMS surface with the carboxylate-terminated AuNSs exhibit an invariant extinction spectrum profile with broad surface plasmon resonance peaks that are notably still centered at ~800 nm (see Figure S9 in the Supporting Information). These data indicate that the process of surface modification, while producing surfaces that exhibit limited levels of nanoshell clustering, exerts little influence on the light absorption/scattering characteristics of the AuNSs and, presumably, the associated photothermal properties.

Bacterial Adherence Assay of Pathogenic *E. faecalis*. Pathogenic *E. faecalis* bacteria were used to demonstrate the photothermal impact of our model catheter surfaces modified with AuNSs upon exposure to a NIR laser. *E. faecalis* are Gram-positive cocci that typically grow into structures that consist of

DOI: 10.1021/am506516r
ACS Appl. Mater. Interfaces 2015, 7, 3981−3993

dimers or oligomers arranged in short chains.[52] The cell wall of *E. faecalis* is comprised of three main components: peptidoglycan, teichoic acid, and polysaccharides. *E. faecalis* show an overall negative charge due to the presence of phosphodiester bonds between teichoic acid monomers. With the negative charge on their cell walls, *E. faecalis* might prefer to adhere on positively charged surfaces. Note, however, that the carboxylic acid-functionalized AuNSs used for modifying the PAMAM-coated surface possess a negative surface charge.

To confirm that our AuNS-modified surfaces can be used as a platform for attachment of *E. faecalis* in the photothermal assay, we exposed the bacteria to the PAMAM and AuNS-modified surfaces by incubating all surfaces in a 10^8 CFU/mL concentration of *E. faecalis* for 120 h at 37 °C. The results were evaluated using an optical microscope, and selected bright-field images are shown in Figure 4. Surprisingly, the

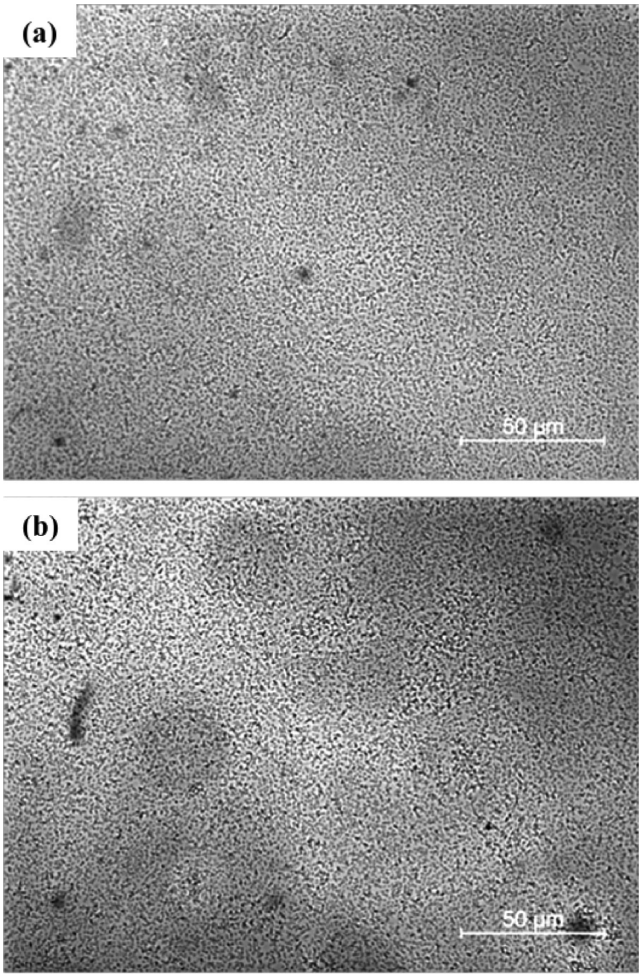

Figure 4. Reflected bright-field images of *E. faecalis* obtained after an incubation period of 120 h for (a) a PAMAM surface and (b) a AuNS-modified PDMS surface.

results for the AuNS-modified PDMS surfaces showed no substantial difference from the PAMAM surfaces that present positive charges on their surfaces. Moreover, these images show the distribution of *E. faecalis* cells on both surfaces produced a surface coverage of ~70%. Nevertheless, these results demonstrate that the relatively long-term duration of the bacterial adherence allows the *E. faecalis* to cover the AuNS-coated surfaces, regardless of the initial charged state of the surfaces, and this model can be further used in the targeted photothermal studies. Indeed, a wide variety of coatings based on antibacterial agents, such as antibiotics and silver particles, have been reported that prevent or reduce pathogenic biofilm formation over the short term under nutrient-deficient conditions.[53,54] However, such coatings fail to work well over the long term in nutrient-rich environments, such as urine, in which the bacteria grow rapidly and secrete substances that fully neutralize and/or cover the antimicrobial surface, rendering it incapable of preventing bacterial adhesion and biofilm formation.[55,56]

Photothermal Effects of AuNS-Modified PDMS Surfaces against *E. faecalis*. After successfully generating AuNS-modified surfaces that have the capability to interact with *E. faecalis*, these model catheter surfaces were tested as platforms for photothermally killing pathogenic bacteria. The photothermal killing process was undertaken using several different time intervals under illumination with an 810-nm NIR diode laser to determine the time frame required to produce sufficient exposure to bacteria-killing heat. To prepare four sets of three surface samples, we incubated small strips (0.3 cm × 1 cm) of both types of functionalized AuNS-modified PDMS surfaces (16-MHDA- and lipoic acid-functionalized AuNSs), along with a control sample produced with PAMAM on the PDMS surface in the absence of the AuNSs, with *E. faecalis* at 37 °C for 120 h. Three of these sets of samples were then exposed to laser illumination for 5, 7, and 10 min, respectively, with the fourth sample set not receiving any laser exposure.

The presence of surviving bacteria on these surfaces was evaluated by colony formation assay, where the bacteria were detached from the surfaces by sonication in 0.01% SDS solution and subsequently vortexed for 2 min at 2000 rpm. The resulting bacterial suspension was serially diluted before plating in duplicate on LB agar, and the bacterial colonies formed were counted after 24 h of incubation at 37 °C. We developed this protocol and have validated that the viability of the bacteria detached using our method remains unchanged, and <1% of the bacteria are left on the surface after subjecting the samples to the SDS solution/sonication protocol (see Figures S10 and S11 in the Supporting Information). The visual images from the colony formation assays from our AuNS-modified PDMS surfaces before and after exposure to NIR light and the bar graphs corresponding to the average of the colonies formed from four experiments performed in duplicate are shown in Figure 5. NIR illumination for 5 min shows that the surviving *E. faecalis* were substantially diminished when compared to the control sample. The results after 10 min of laser exposure were even more convincing. This outcome is exciting, because it implies that our hyperthermia approach is effective against the colonization of a pathogen, providing an alternative method for fighting antibiotic-resistant bacteria. The decrease in the number of bacterial colonies is believed to reflect NIR irradiation-induced damage, where the heat created by this photothermal approach is sufficient to kill the bacteria on our model catheter surfaces. It should be noted that the AuNSs functionalized with two different carboxylate-terminated organosulfur ligands produced statistically equivalent results.

To confirm that the photothermal heating protocol effectively kills bacteria on AuNS-modified PDMS surfaces, we used SEM to examine the morphology of the bacteria before and after exposure of the surface to NIR light for 10 min. As shown in Figure 6, the SEM image of the surface exposed to NIR light reveals that localized overheating generated by the

DOI: 10.1021/am506516r
ACS Appl. Mater. Interfaces 2015, 7, 3981−3993

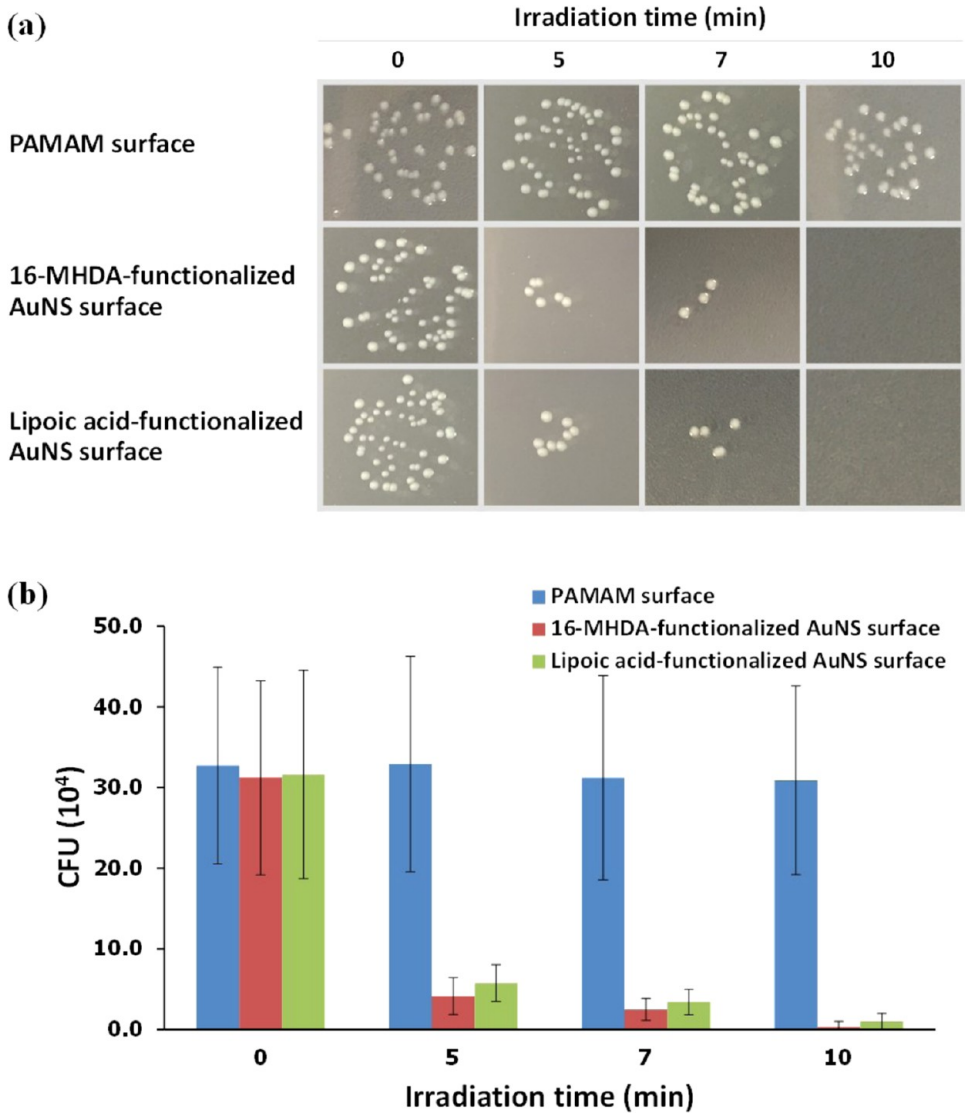

Figure 5. Results from the colony formation assays of the surviving *E. faecalis* after NIR irradiation in the form of (a) visual images of bacterial colonies from PAMAM- and AuNS-modified PDMS surfaces after NIR irradiation for the exposure times indicated and (b) bar graphs corresponding to the average of the bacterial colonies formed from four independent experiments (CFU; colony forming unit).

SPR response of the AuNSs led to thermal decomposition and rupturing of the cell wall of the pathogenic *E. faecalis*. These results demonstrate that with a radiation time of 10 min, thermal diffusion from the AuNSs can lead to heat-induced damage to bacteria located in close proximity to the AuNSs.

To verify that the rupturing of the bacteria cell walls could be attributed to changes in thermal energy, we evaluated the photothermal properties of a AuNS-modified PDMS surface by utilizing thermal imaging to monitor spatially resolved temperature changes due to NIR light harvesting and heat generation (see Figure 7). The results show that the AuNS-modified PDMS surface can effectively cause a significant surface temperature rise after NIR illumination. The average temperature obtained from the entire AuNS-modified PDMS surface (1 cm × 1 cm) increased from an initial temperature of 22.1 ± 0.4 °C to 73.0 ± 4.7 °C, after NIR illumination for 10 min. Our photothermal heating results are similar to a previous report by Yella et al., which examined the temperature distribution and evolution in gold nanoshell-populated phantom tissues.[57] In their studies, the temperature of the environment surrounding the AuNSs increased rapidly as a result of strong heat production by the gold nanoshells, which was generated from the absorbed laser energy under localized surface plasmon resonance conditions. However, without nanoshell-mediated resonance absorption and heating, the temperature increase was practically negligible.

Several *in vivo* studies have demonstrated the efficacy of nanoshells for the treatment of tumors through targeted photothermal destruction by the accumulation of NIR-responsive AuNSs at tumor sites.[20,22] In the study by O'Neal et al.,[20] the surface temperature at the tumor site was increased to ∼50 °C after the tumor was exposed to NIR light at 4 W/cm^2 for 3 min. Hirsch et al.[22] conducted a study of the temperature distribution of tumors in mice during thermal therapy by using magnetic resonance temperature imaging. They reported the temperature change for the AuNS-treated tumors to be 37.4 ± 6.6 °C, which is a temperature increase that was sufficiently high to cause irreversible thermal damage to the tumor, while the temperature increase in the nanoshell-free control group was only 9.1 ± 4.7 °C.

DOI: 10.1021/am506516r
ACS Appl. Mater. Interfaces 2015, 7, 3981−3993

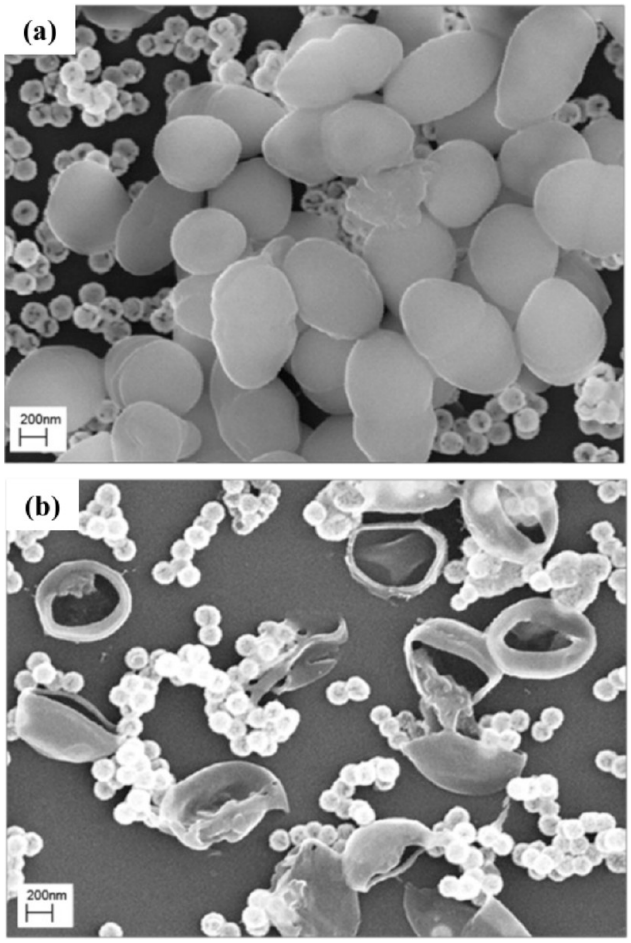

Figure 6. SEM images of *E. faecalis* on AuNS-modified PDMS surfaces (a) before and (b) after NIR exposure.

It is widely assumed that the efficacy of a thermal treatment is given by the magnitude of the incremental temperature increase (above biological norms) and the duration.[58] Regarding the magnitude of the induced incremental temperature increase, a treatment that produces irreversible tissue damage has been shown to be carried out successfully by increasing the temperature of cells above 50 °C, and the activation of cell death is achieved as a result of a coagulative necrosis process.[59,60] Irreversible thermal treatments have clinical applications beyond cancer; in urology, such treatments are used for benign prostatic hyperplasia,[61] and in cardiology, such treatments are used for thermal angioplasty.[62] Most proteins experience instantaneous and irreversible denaturation above 60 °C, while higher temperatures (above 80 °C) lead to tissue rupture due to water vaporization.[63]

For this report, we showed that a PDMS surface modified with AuNSs under NIR irradiation produced a significant incremental temperature increase and a localized surface temperature of ∼73 °C, leading to bacterial cell death. We believe that the damage to these bacterial cells arises from the rapid conversion of absorbed light by the gold nanostructure to localized thermal energy, which heats and ruptures the cell walls. The process has been described by Link et al. as involving the transfer of absorbed light from gold nanostructures to cells by rapid electron−phonon relaxation in the nanoparticles, followed by phonon−phonon relaxation,[64] leading to an increase in the temperature of the nanoparticles and nearby cells. However, thermally and mechanically induced compromising of cell membrane integrity also has been reported to be a leading cause of cell photothermal damage.[65] The photothermolysis mechanism of NIR plasmonic photothermal therapy with continuous-wave lasers and gold nanostructures has shown that laser energy used to destroy the cells when the nanoparticles are located on the cytoplasm membrane is 10 times lower than that required when the nanoparticles are internalized inside the cytoplasm.

Photothermally induced cell death can take place via apoptosis or necrosis, depending on the dosage, type, and time of irradiation. It is also dependent on the subcellular location of the gold nanostructures when they are located inside a cell. In a study using pulsed laser irradiation, intermittent laser exposure induced cell damage via a series of photothermal and accompanied phenomena: denaturation or breakdown of proteins, cell cavitation, cellular structure rupturing, evaporation of cellular liquid, and bubble formation by shock waves due to particle thermal expansion, evaporation, or plasma generation associated with the gold nanostructures.[66] Although prior studies have shown the effectiveness of gold nanoparticle-mediated photothermal disruption of cellular structures,[65−69] our results demonstrate that AuNSs can be used to photothermally induce cell rupturing that efficiently kills bacteria.

CONCLUSIONS

This study has demonstrated an effective photothermal approach to destroy pathogenic bacteria (*E. faecalis*) within a short period of time (5−10 min), using an *in vitro* test on PDMS model catheter surfaces. The AuNS-modified surfaces, combined with NIR irradiation, can be viewed as a potential broad-spectrum antibiotic that rapidly kills adhered pathogens upon treatment. This method relies upon the generation of heat by AuNSs in response to NIR irradiation and the transfer

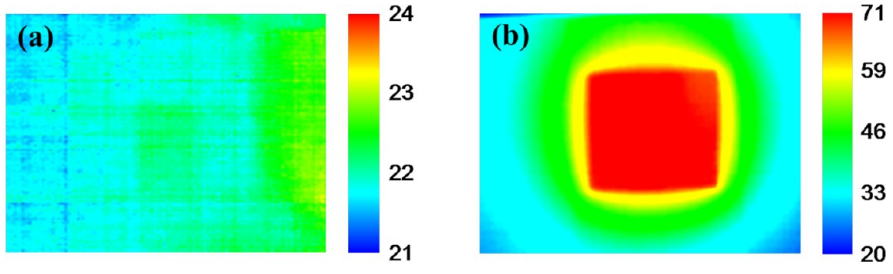

Figure 7. Thermal imaging temperature maps used to demonstrate photothermal heating of the AuNS-modified PDMS surface (a) before and (b) after exposure to NIR light for 10 min.

DOI: 10.1021/am506516r
ACS Appl. Mater. Interfaces 2015, 7, 3981−3993

of thermal energy to the bacteria. This hyperthermia approach might potentially become a new adjuvant therapeutic method for use in applications where the NIR light can effectively reach the surface of the catheter. For our current system, the wavelength of the NIR light used was 810 nm, which can penetrate human tissue up to 3 or 4 mm, depending on the laser strength and optical scattering by the tissue involved. To enhance the effectiveness of this therapeutic approach, additional research is needed to optimize the absorption maxima of the AuNSs and the associated NIR laser wavelength and power used, with an ultimate goal of utilizing NIR light penetration for the treatment of catheters *in situ*.

■ ASSOCIATED CONTENT

Supporting Information

Included are EDX data, supplemental XPS and UV−vis extinction spectra, additional SEM and reflected bright-field images, and validation of the method used for detachment of the bacteria. This material is available free of charge via the Internet at http://pubs.acs.org/.

■ AUTHOR INFORMATION

Corresponding Authors

*E-mail: cai@uh.edu (C. Cai).
*E-mail: trlee@uh.edu (T. R. Lee).

Notes

The authors declare no competing financial interest.

■ ACKNOWLEDGMENTS

We thank the Robert A. Welch Foundation (Grant No. E-1320), the National Science Foundation (Grant No. DMR-1207583), and the Texas Center for Superconductivity, for providing generous support for this research.

■ REFERENCES

(1) Raad, I.; Hanna, H. Intravascular Catheters Impregnated with Antimicrobial Agents: A Milestone in the Prevention of Bloodstream Infections. *Support. Care Cancer* **1999**, *7*, 386−390.
(2) O'Grady, N. P.; Alexander, M.; Dellinger, E. P.; Gerberding, J. L.; Heard, S. O.; Maki, D. G.; Masur, H.; McCormick, R. D.; Mermel, L. A.; Pearson, M. L.; Raad, I. I.; Randolph, A.; Weinstein, R. A. Guidelines for the Prevention of Intravascular Catheter-Related Infections. *Infect. Control Hosp. Epidemiol.* **2002**, *23*, 759−769.
(3) Maki, D. G.; Kluger, D. M.; Crnich, C. J. The Risk of Bloodstream Infection in Adults with Different Intravascular Devices: A Systematic Review of 200 Published Prospective Studies. *Mayo Clin. Proc.* **2006**, *81*, 1159−1171.
(4) Smith, M. J. Catheter-Related Bloodstream Infections in Children. *Am. J. Infect. Control* **2008**, *36*, S173 e1−S173 e3.
(5) Desai, D. G.; Liao, K. S.; Cevallos, M. E.; Trautner, B. W. Silver or Nitrofurazone Impregnation of Urinary Catheters Has a Minimal Effect on Uropathogen Adherence. *J. Urol.* **2010**, *184*, 2565−2571.
(6) Ha, U.-S.; Cho, Y.-H. Catheter-Associated Urinary Tract Infections: New Aspects of Novel Urinary Catheters. *Int. J. Antimicrob. Agents* **2006**, *28*, 485−490.
(7) Jacobsen, S. M.; Stickler, D. J.; Mobley, H. L. T.; Shirtliff, M. E. Complicated Catheter-Associated Urinary Tract Infections Due to *Escherichia coli* and *Proteus mirabilis*. *Clin. Microbiol. Rev.* **2008**, *21*, 26−59.
(8) Tambyah, P. A. Catheter-Associated Urinary Tract Infections: Diagnosis and Prophylaxis. *Int. J. Antimicrob. Agents* **2004**, *24S*, S44−S48.
(9) Davey, M. E.; O'Toole, G. A. Microbial Biofilms: from Ecology to Molecular Genetics. *Microbiol. Mol. Biol. Rev.* **2000**, *64*, 847−867.
(10) Harding, G. K. M.; Zhanel, G. G.; Nicolle, L. E.; Cheang, M. Antimicrobial Treatment in Diabetic Women with Asymptomatic Bacteriuria. *N. Engl. J. Med.* **2002**, *347*, 1576−1583.
(11) Trautner, B. W.; Darouiche, R. O. Role of Biofilm in Catheter-Associated Urinary Tract Infection. *Am. J. Infect. Control* **2004**, *32*, 177−183.
(12) Knetsch, M. L. W.; Koole, L. H. New Strategies in the Development of Antimicrobial Coatings: The Example of Increasing Usage of Silver and Silver Nanoparticles. *Polymers* **2011**, *3*, 340−366.
(13) Mukherjee, S. G.; O'Claonadh, N.; Casey, A.; Chambers, G. Comparative *In Vitro* Cytotoxicity Study of Silver Nanoparticle on Two Mammalian Cell Lines. *Toxicol. In Vitro* **2012**, *26*, 238−251.
(14) Peng, H.; Zhang, X. H.; Wei, Y.; Liu, W. T.; Li, S. L.; Yu, G. Y.; Fu, X.; Cao, T.; Deng, X. L. Cytotoxicity of Silver Nanoparticles in Human Embryonic Stem Cell-Derived Fibroblasts and an L-929 Cell Line. *J. Nanomater.* **2012**, *2012*, 160145.
(15) Pratsinis, A.; Hervella, P.; Leroux, J.-C.; Pratsinis, S. E.; Sotiriou, G. A. Toxicity of Silver Nanoparticles in Macrophages. *Small* **2013**, *9*, 2576−2584.
(16) Pham, T.; Jackson, J. B.; Halas, N. J.; Lee, T. R. Preparation and Characterization of Gold Nanoshells Coated with Self-Assembled Monolayers. *Langmuir* **2002**, *18*, 4915−4920.
(17) Kim, J.-H.; Bryan, W. W.; Lee, T. R. Preparation, Characterization, and Optical Properties of Gold, Silver, and Gold−Silver Alloy Nanoshells Having Silica Cores. *Langmuir* **2008**, *24*, 11147−11152.
(18) Erickson, T. A.; Tunnell, J. W. Gold Nanoshells in Biomedical Applications. In *Nanomaterials for the Life Sciences: Mixed Metal Nanomaterials*; Kumar, C. S. S. R., Ed.; Wiley: New York, 2009.
(19) Gad, S. C.; Sharp, K. L.; Montgomery, C.; Payne, J. D.; Goodrich, G. P. Evaluation of the Toxicity of Intravenous Delivery of Auroshell Particles (Gold−Silica Nanoshells). *Int. J. Toxicol.* **2012**, *31*, 584−594.
(20) O'Neal, D. P.; Hirsch, L. R.; Halas, N. J.; Payne, J. D.; West, J. L. Photo-Thermal Tumor Ablation in Mice Using Near Infrared-Absorbing Nanoparticles. *Cancer Lett.* **2004**, *209*, 171−176.
(21) Weissleder, R. A Clearer Vision for *In Vivo* Imaging. *Nat. Biotechnol.* **2001**, *19*, 316−317.
(22) Hirsch, L. R.; Stafford, R. J.; Bankson, J. A.; Sershen, S. R.; Rivera, B.; Price, R. E.; Hazle, J. D.; Halas, N. J.; West, J. L. Nanoshell-Mediated Near-Infrared Thermal Therapy of Tumors Under Magnetic Resonance Guidance. *Proc. Natl. Acad. Sci. U.S.A.* **2003**, *100*, 13549−13554.
(23) Khlebtsov, B.; Zharov, V.; Melnikov, A.; Tuchin, V.; Khlebtsov, N. Optical Amplification of Photothermal Therapy with Gold Nanoparticles and Nanoclusters. *Nanotechnology* **2006**, *17*, 5167−5179.
(24) Chen, K.; Soto, I.; Monroe, W. T.; Alexander, J. S. Photothermolysis of Lymphatic Endothelial Cells by Gold Nanoshell-Mediated Hyperthermia. *J. Nanosci. Nanotechnol.* **2014**, *14*, 5347−5354.
(25) Dickerson, E. B.; Dreaden, E. C.; Huang, X. H.; El-Sayed, I. H.; Chu, H. H.; Pushpanketh, S.; McDonald, J. F.; El-Sayed, M. A. Gold Nanorod Assisted Near-Infrared Plasmonic Photothermal Therapy (PPTT) of Squamous Cell Carcinoma in Mice. *Cancer Lett.* **2008**, *269*, 57−66.
(26) Tuchina, E. S.; Petrov, P. O.; Kozina, K. V.; Ratto, F.; Centi, S.; Pini, R.; Tuchin, V. V. Using Gold Nanorods Labelled with Antibodies Under the Photothermal Action of NIR Laser Radiation on *Staphylococcus aureus*. *Quantum Electron.* **2014**, *44*, 683−688.
(27) Hu, B.; Wang, N.; Han, L.; Chen, M.-L.; Wang, J.-H. Core-Shell-Shell Nanorods for Controlled Release of Silver that Can Serve as a Nanoheater for Photothermal Treatment on Bacteria. *Acta Biomater.* **2015**, *11*, 511−519.
(28) Lopez, A. I.; Kumar, A.; Planas, M. R.; Li, Y.; Nguyen, T. V.; Cai, C. Biofunctionalization of Silicone Polymers Using Poly(amidoamine) Dendrimers and a Mannose Derivative for Prolonged Interference Against Pathogen Colonization. *Biomaterials* **2011**, *32*, 4336−4346.

DOI: 10.1021/am506516r
ACS Appl. Mater. Interfaces 2015, 7, 3981−3993

(29) Emori, T. G.; Gaynes, R. P. An Overview of Nosocomial Infections, Including the Role of the Microbiology Laboratory. *Clin. Microbiol. Rev.* **1993**, *6*, 428−442.
(30) Liang, Z. S.; Liu, Y.; Ng, S. S.; Li, X. Y.; Lai, L. H.; Luo, S. F.; Liu, S. Y. The Effect of pH Value on the Formation of Gold Nanoshells. *J. Nanopart. Res.* **2011**, *13*, 3301−3311.
(31) Stöber, W.; Fink, A.; Bohn, E. Controlled Growth of Monodisperse Silica Spheres in the Micron Size Range. *J. Colloid Interface Sci.* **1968**, *26*, 62−69.
(32) Westcott, S. L.; Oldenburg, S. J.; Lee, T. R.; Halas, N. J. Formation and Adsorption of Clusters of Gold Nanoparticles onto Functionalized Silica Nanoparticle Surfaces. *Langmuir* **1998**, *14*, 5396−5401.
(33) Duff, D. G.; Baiker, A.; Edwards, P. P. A New Hydrosol of Gold Clusters. 1. Formation and Particle Size Variation. *Langmuir* **1993**, *9*, 2301−2309.
(34) Corradi, A. B.; Bondioli, F.; Ferrari, A. M.; Focher, B.; Leonelli, C. Synthesis of Silica Nanoparticles in a Continuous-Flow Microwave Reactor. *Powder Technol.* **2006**, *167*, 45−48.
(35) Tsagkogeorgas, F.; Ochsenkuhn-Petropoulou, M.; Niessner, R.; Knopp, D. Encapsulation of Biomolecules for Bioanalytical Purposes: Preparation of Diclofenac Antibody-Doped Nanometer-Sized Silica Particles by Reverse Micelle and Sol−Gel Processing. *Anal. Chim. Acta* **2006**, *573*−*574*, 133−137.
(36) Lim, H. M.; Lee, J.; Jeong, J.-H.; Oh, S.-G.; Lee, S.-H. Comparative Study of Various Preparation Methods of Colloidal Silica. *Engineering* **2010**, *2*, 998−1005.
(37) Jang, H. D.; Chang, H.; Suh, Y.; Okuyama, K. Synthesis of SiO_2 Nanoparticles from Sprayed Droplets of Tetraethylorthosilicate by the Flame Spray Pyrolysis. *Curr. Appl. Phys.* **2006**, *6S1*, e110−e113.
(38) Grabar, K. C.; Allison, K. J.; Baker, B. E.; Bright, R. M.; Brown, K. R.; Freeman, R. G.; Fox, A. P.; Keating, C. D.; Musick, M. D.; Natan, M. J. Two-Dimensional Arrays of Colloidal Gold Particles: A Flexible Approach to Macroscopic Metal Surfaces. *Langmuir* **1996**, *12*, 2353−2361.
(39) Wang, X.-D.; Shen, Z.-X.; Sang, T.; Cheng, X.-B.; Li, M.-F.; Chen, L.-Y.; Wang, Z.-S. Preparation of Spherical Silica Particles by Stober Process with High Concentration of Tetra-ethyl-orthosilicate. *J. Colloid Interface Sci.* **2010**, *341*, 23−29.
(40) Badley, R. D.; Ford, W. T.; McEnroe, F. J.; Assink, R. A. Surface Modification of Colloidal Silica. *Langmuir* **1990**, *6*, 792−801.
(41) Oldenburg, S. J.; Averitt, R. D.; Westcott, S. L.; Halas, N. J. Nanoengineering of Optical Resonances. *Chem. Phys. Lett.* **1998**, *288*, 243−247.
(42) Cano, E.; Torres, C. L.; Bastidas, J. M. An XPS Study of Copper Corrosion Originated by Formic Acid Vapour at 40% and 80% Relative Humidity. *Mater. Corros.* **2001**, *52*, 667−676.
(43) Brinson, B. E.; Lassiter, J. B.; Levin, C. S.; Bardhan, R.; Mirin, N.; Halas, N. J. Nanoshells Made Easy: Improving Au Layer Growth on Nanoparticle Surfaces. *Langmuir* **2008**, *24*, 14166−14171.
(44) Lee, H. J.; Jamison, A. C.; Yuan, Y. H.; Li, C.-H.; Rittikulsittichai, S.; Rusakova, I.; Lee, T. R. Robust Carboxylic Acid-Terminated Organic Thin Films and Nanoparticle Protectants Generated from Bidentate Alkanethiols. *Langmuir* **2013**, *29*, 10432−10439.
(45) Miura, Y.; Kimura, S.; Imanishi, Y.; Umenmura, J. Formation of Oriented Helical Peptide Layers on a Gold Surface Due to the Self-Assembling Properties of Peptides. *Langmuir* **1998**, *14*, 6935−6940.
(46) Wang, K.; Jiang, D. C.; Kong, J. L.; Zhang, S.; Liu, B. H.; Lu, T. P. Sensitively Detecting Recombinant Hirudin Variant-2 with Capacitive Immunoassay Based on Self-Assembled Monolayers. *Anal. Lett.* **2003**, *36*, 2571−2583.
(47) Karamanska, R.; Mukhopadhyay, B.; Russell, D. A.; Field, R. A. Thioctic Acid Amides: Convenient Tethers for Achieving Low Nonspecific Protein Binding to Carbohydrates Presented on Gold Surfaces. *Chem. Commun.* **2005**, *26*, 3334−3336.
(48) Hahn, C. D.; Leitner, C.; Weinbrenner, T.; Schlapak, R.; Tinazli, A.; Tampé, R.; Lackner, B.; Steindl, C.; Hinterdorfer, P.; Gruber, H. J.; Hölzl, M. Self-Assembled Monolayers with Latent Aldehydes for Protein Immobilization. *Bioconjugate Chem.* **2007**, *18*, 247−253.
(49) Castner, D. G.; Hinds, K.; Grainger, D. W. X-ray Photoelectron Spectroscopy Sulfur 2p Study of Organic Thiol and Disulfide Binding Interactions with Gold Surfaces. *Langmuir* **1996**, *12*, 5083−5086.
(50) Willey, T. M.; Vance, A. L.; Bostedt, C.; van Buuren, T.; Meulenberg, R. W.; Terminello, L. J.; Fadley, C. S. Surface Structure and Chemical Switching of Thioctic Acid Adsorbed on Au(111) as Observed Using Near-Edge X-ray Absorption Fine Structure. *Langmuir* **2004**, *20*, 4939−4944.
(51) Stiriba, S.-E.; Frey, H.; Haag, R. Dendritic Polymers in Biomedical Applications: From Potential to Clinical Use in Diagnostics and Therapy. *Angew. Chem., Int. Ed.* **2002**, *41*, 1329−1334.
(52) DelaMaza, L. M.; Peterson, E. M.; Pezzlo, M. T.; Shigei, J. T. *Color Atlas of Medical Bacteriology*; ASM Press: Washington, DC, 2004.
(53) Novikov, A.; Lam, M. Y.; Mermel, L. A.; Casey, A. L.; Elliott, T. S.; Nightingale, P. Impact of Catheter Antimicrobial Coating on Species-Specific Risk of Catheter Colonization: A Meta-Analysis. *Antimicrob. Resist. Infect. Control* **2012**, *1*, 40.
(54) Drekonja, D. M.; Kuskowski, M. A.; Wilt, T. J.; Johnson, J. R. Antimicrobial Urinary Catheters: A Systematic Review. *Expert Rev. Med. Devices* **2008**, *5*, 495−506.
(55) Karchmer, T. B.; Giannetta, E. T.; Muto, C. A.; Strain, B. A.; Farr, B. M. A Randomized Crossover Study of Silver-Coated Urinary Catheters in Hospitalized Patients. *Arch. Int. Med.* **2000**, *160*, 3294−3298.
(56) Regev-Shoshani, G.; Ko, M.; Crowe, A.; Av-Gay, Y. Comparative Efficacy of Commercially Available and Emerging Antimicrobial Urinary Catheters Against Bacteriuria Caused by *E. coli In Vitro*. *Urology* **2011**, *78*, 334−339.
(57) Yella, A.; Li, B. Q.; Mohanty, P.; Liu, C. Measurement of Temperature Distribution and Evolution During Surface Plasma Resonance Heating of Gold Nanoshells-Embedded Phantom Tissue. *Exp. Therm. Fluid Sci.* **2013**, *47*, 34−39.
(58) Habash, R. W. Y.; Bansal, R.; Krewski, D.; Alhafid, H. T. Thermal Therapy, Part 2: Hyperthermia Techniques. *Crit. Rev. Biomed. Eng.* **2006**, *34*, 491−542.
(59) Chakravarty, P.; Marches, R.; Zimmerman, N. S.; Swafford, A. D.-E.; Bajaj, P.; Musselman, I. H.; Pantano, P.; Draper, R. K.; Vitetta, E. S. Thermal Ablation of Tumor Cells with Antibody-Functionalized Single-Walled Carbon Nanotubes. *Proc. Natl. Acad. Sci. U. S. A.* **2008**, *105*, 8697−8702.
(60) Habash, R. W. Y.; Bansal, R.; Krewski, D.; Alhafid, H. T. Thermal Therapy, Part III: Ablation Techniques. *Crit. Rev. Biomed. Eng.* **2007**, *35*, 37−121.
(61) Corwin, T.; Lindberg, G.; Traxer, O.; Gettman, M. T.; Smith, T. G.; Pearle, M. S.; Cadeddu, J. A. Laparoscopic Radiofrequency Thermal Ablation of Renal Tissue with and without Hilar Occlusion. *J. Urol.* **2001**, *166*, 281−284.
(62) Litvack, F.; Grundfest, W. S.; Papaioannou, T.; Mohr, F. W.; Jakubowski, A. T.; Forrester, J. S. Role of Laser and Thermal Ablation Devices in the Treatment of Vascular Diseases. *Am. J. Cardiol.* **1988**, *61*, 81G−86G.
(63) Welch, A. J.; Motamedi, M.; Rastegar, S.; LeCarpentier, G. L.; Jansen, D. Laser Thermal Ablation. *Photochem. Photobiol.* **1991**, *53*, 815−823.
(64) Link, S.; El-Sayed, M. A. Shape and Size Dependence of Radiative, Non-Radiative and Photothermal Properties of Gold Nanocrystals. *Int. Rev. Phys. Chem.* **2000**, *19*, 409−453.
(65) Tong, L.; Zhao, Y.; Huff, T. B.; Hansen, M. N.; Wei, A.; Cheng, J.-X. Gold Nanorods Mediate Tumor Cell Death by Compromising Membrane Integrity. *Adv. Mater.* **2007**, *19*, 3136−3141.
(66) Pustovalov, V. K.; Smetannikov, A. S.; Zharov, V. P. Photothermal and Accompanied Phenomena of Selective Nanophotothermolysis with Gold Nanoparticles and Laser Pulses. *Laser Phys. Lett.* **2008**, *5*, 775−792.
(67) Zharov, V. P.; Mercer, K. E.; Galitovskaya, E. N.; Smeltzer, M. S. Photothermal Nanotherapeutics and Nanodiagnostics for Selective

DOI: 10.1021/am506516r
ACS Appl. Mater. Interfaces 2015, 7, 3981−3993

Killing of Bacteria Targeted with Gold Nanoparticles. *Biophys. J.* **2006**, *90*, 619−627.
(68) Kim, C.-B.; Yi, D. K.; Kim, P. S. S.; Lee, W.; Kim, M. J. Rapid Photothermal Lysis of the Pathogenic Bacteria, *Escherichia Coli* Using Synthesis of Gold Nanorods. *J. Nanosci. Nanotechnol.* **2009**, *9*, 2841−2845.
(69) Tong, L.; Cheng, J.-X. Gold Nanorod-Mediated Photothermolysis Induces Apoptosis of Macrophages via Damage of Mitochondria. *Nanomedicine* **2009**, *4*, 265−276.

DOI: 10.1021/am506516r
ACS Appl. Mater. Interfaces 2015, 7, 3981−3993